

UCSF

UC San Francisco Previously Published Works

Title

SARAF Luminal Domain Structure Reveals a Novel Domain-Swapped β -Sandwich Fold Important for SOCE Modulation

Permalink

<https://escholarship.org/uc/item/3m8218j3>

Journal

Journal of Molecular Biology, 431(15)

ISSN

0022-2836

Authors

Kimberlin, Christopher R

Meshcheriakova, Anna

Palty, Raz

et al.

Publication Date

2019-07-01

DOI

10.1016/j.jmb.2019.05.008

Peer reviewed



Published in final edited form as:

J Mol Biol. 2019 July 12; 431(15): 2869–2883. doi:10.1016/j.jmb.2019.05.008.

SARAF luminal domain structure reveals a novel domain-swapped β -sandwich fold important for SOCE modulation

Christopher R. Kimberlin^{1,#}, Anna Meshcheriakova^{2,#}, Raz Palty³, Adi Raveh², Izhar Karbat², Eitan Reuveny^{2,*}, and Daniel L. Minor, Jr.^{1,4,5,6,7,*}

¹Cardiovascular Research Institute, University of California, San Francisco, California 93858-2330 USA

²Department of Biomolecular Sciences, Weizmann Institute of Science, Rehovot, Israel 7610001

³Rappaport Family School of Medicine, Technion-Israel Institute of Technology, Haifa, Israel 31096

⁴Departments of Biochemistry and Biophysics, and Cellular and Molecular Pharmacology, University of California, San Francisco, California 93858-2330 USA

⁵California Institute for Quantitative Biomedical Research, University of California, San Francisco, California 93858-2330 USA

⁶Kavli Institute for Fundamental Neuroscience, University of California, San Francisco, California 93858-2330 USA

⁷Molecular Biophysics and Integrated Bioimaging Division, Lawrence Berkeley National Laboratory, Berkeley, CA 94720 USA

Abstract

Store Operated Calcium Entry (SOCE) plays key roles in cell proliferation, muscle contraction, immune responses, and memory formation. The coordinated interactions of a number of proteins from the plasma and endoplasmic reticulum (ER) membranes control SOCE to replenish internal Ca^{2+} stores and generate intracellular Ca^{2+} signals. SARAF, an ER resident component of the SOCE pathway having no homology to any characterized protein, serves as an important brake on

*Correspondence to: daniel.minor@ucsf.edu and e.reuveny@weizmann.ac.il.

#equal contributions

Author Contributions

C.K., A.M., E.R., and D.L.M. conceived the study and designed the experiments. C.K. cloned, expressed, purified, crystalized, and determined the structure of SARAF_L and variants and performed biochemical and biophysical characterization experiments. A.M., R.P. and A.R. performed electrophysiology and imaging experiments. A.M., R.P., A.R., I. K. and E.R. analyzed the imaging and electrophysiology data. A.M. performed molecular biology experiments. E.R. and D.L.M analyzed data and provided guidance and support. C.K., A.M., R.P, E.R. and D.L.M. wrote the paper.

Publisher's Disclaimer: This is a PDF file of an unedited manuscript that has been accepted for publication. As a service to our customers we are providing this early version of the manuscript. The manuscript will undergo copyediting, typesetting, and review of the resulting proof before it is published in its final citable form. Please note that during the production process errors may be discovered which could affect the content, and all legal disclaimers that apply to the journal pertain.

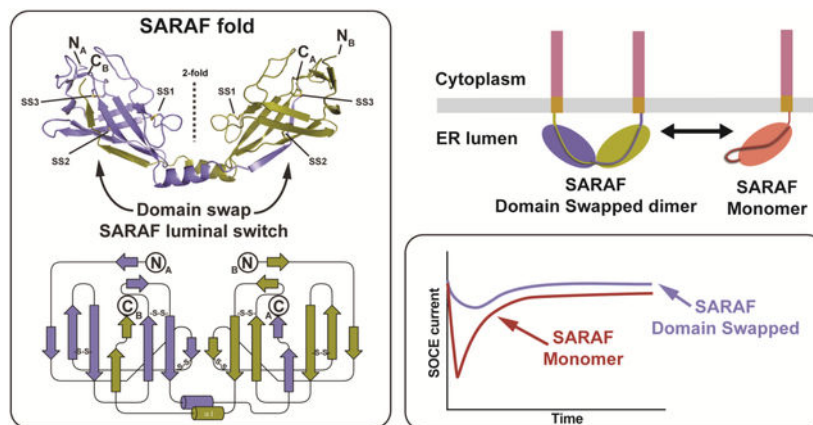
Accession numbers: Coordinates and structure factors for SARAF_L, SARAF_LSS Monomer, and SARAF_LSS Dimer are deposited with the RCSB under accession codes 6O2U, 6O2V, and 6O2W, respectively, and will be released immediately upon publication.

Declaration of Interests

The authors declare no competing interests.

SOCE. Here, we describe the X-ray crystal structure of the SARAF luminal domain, SARAF_L. This domain forms a novel ten-stranded β -sandwich fold that includes a set of three conserved disulfide bonds, denoted the ‘SARAF-fold’. The structure reveals a domain-swapped dimer in which the last two β -strands (β_9 and β_{10}) are exchanged forming a region denoted the ‘SARAF luminal switch’ that is essential for dimerization. Sequence comparisons reveal that the SARAF-fold is highly conserved in vertebrates and in a variety of pathologic fungi. Förster Resonance Energy Transfer (FRET) experiments using full-length SARAF validate the formation of the domain-swapped dimer in cells and demonstrate that dimerization is reversible. A designed variant lacking the SARAF luminal switch shows that the domain swapping is essential to function and indicates that the SARAF dimer accelerates SOCE inactivation.

Graphical Abstract



Keywords

Store operated calcium entry (SOCE); SARAF; X-ray crystallography; Domain swapping, β -sandwich fold, electrophysiology

Calcium is a potent second messenger required for diverse cellular signaling processes that occur over a wide range of timescales such as vesicle release (μ s), fertilization (minutes), and proliferation and apoptosis (hours) [1, 2]. Consequently, cells use a multitude of systems to control cytoplasmic Ca^{2+} level changes. Signalling in both non-excitabile and excitable cells is frequently initiated by stimulation of a G-protein coupled receptors and receptor tyrosine kinases [3, 4] that trigger inositol triphosphate (IP_3)-mediated release of Ca^{2+} from intracellular stores. The resulting intracellular Ca^{2+} store depletion activates a process called Store Operated Calcium Entry (SOCE) that works to replenish the internal Ca^{2+} stores and that affects a range of responses, such as proliferation, transcription, and cell motility [5–9].

The prototypical mediator of SOCE is the calcium release-activated calcium (CRAC) channel formed by the plasma membrane (PM) pore-forming subunit, Orai, and an endoplasmic reticulum (ER) Ca^{2+} sensor and channel activator, STIM [10–13]. Both SOCE components have multiple isoforms of which the best studied are STIM1 and Orai1. SOCE activation involves an elegant mechanism that results in the clustering of both STIM and

Orai at the ER-PM junctions [14–16]. Depletion of ER Ca^{2+} induces STIM1 oligomerization and translocation to the ER-PM junctions, where it binds to Orai1 and initiates Ca^{2+} influx [17–22]. Once SOCE is initiated, Ca^{2+} from CRAC channels initiates autoregulatory deactivation and inactivation processes that shape the duration and magnitude of the Ca^{2+} signal. Two types of Ca^{2+} dependent inactivation have been described: a fast process that occurs on the millisecond time scale, and a slow process that develops over multiple minutes [23]. The ER resident, single pass transmembrane SARAF [24] (for **SO**CE-**A**ssociated **R**egul**A**Tory **F**actor) is a central facilitator of the slow Ca^{2+} dependent inactivation (SCDI) of CRAC channels.

SARAF lacks homology to any known protein. Previous studies established that the SARAF elements on either side of the membrane encode two distinct functions. The SARAF cytosolic domain is required for driving SOCE inactivation through interaction with STIM [24–26], whereas the luminal domain regulates SOCE inactivation by responding to changes in ER Ca^{2+} levels [24]. Here, we present the X-ray crystal structure of the SARAF ER luminal domain, SARAF_L. This domain forms a domain-swapped dimer arrangement built from a novel β -sandwich fold that we term the ‘SARAF fold’. Cross-linking, analytical ultracentrifugation, and FRET experiments demonstrate that self-association of SARAF_L and full-length SARAF in cells depends upon the domain-swapped element denoted as the ‘SARAF luminal switch’. Finally, CRAC current recording in cells that express wild-type SARAF or dimerization-incompetent SARAF show that self-association via the SARAF luminal switch is critical for control of CRAC currents.

Results

SARAF luminal domain dimerizes using a novel, conserved domain-swapped β -sandwich fold

The SARAF endoplasmic reticulum (ER) luminal domain contains six cysteines and bears no sequence homology to any protein of known structure (Fig. 1a and b). Therefore, we set out to define its structure to gain insight into how it might affect SOCE. Extensive screening identified a human SARAF luminal domain construct that could be expressed in *Escherichia coli* Shuffle Express cells, purified to homogeneity, and crystallized. This construct, denoted SARAF_L, excludes the N-terminal signal peptide, encompasses luminal domain residues 30–164, and ends eight residues before the putative transmembrane helix [24, 27] (Fig. 1a). SARAF_L crystals diffracted X-rays to a resolution of 1.9 Å and the structure was determined by single isomorphous replacement with anomalous scattering (SIRAS) using a single platinum derivative ($\text{K}_2\text{Pt}(\text{NO})_4$) that diffracted X-rays to 2.15 Å (Fig. S1a, Table S1). SARAF_L crystallized with two molecules in the asymmetric unit. One copy had continuous electron density from N- to C-terminus while the other showed short regions of disorder between residues 88–93 and 149–156 (Fig. S1b). Hence, the structural description focuses on the complete copy.

SARAF_L forms a domain swapped dimer comprising a ten β -strand barrel having three conserved disulfides (Fig. 1b–d). There are two well-ordered extended loops that connect β 2– β 4 and β 6– β 8. Both are stabilized by the presence of a short intervening β -strand midway through the loop that forms β -sheet interactions with other β -strands (Fig. 1c and

d). The β 3 strand in the middle of the β 2- β 4 loop makes a parallel β -sheet with β 8, whereas the β 7 strand in the β 6- β 8 loop forms an anti-parallel interaction with β 1. The β 2- β 4 and β 6- β 8 loops are further constrained by the Cys66-Cys73 and Cys114-Cys130 disulfides, respectively. The remaining disulfide, Cys83-Cys97, is buried in the core of the protein and links β 4 and β 5. There is a single β -helix, β 1, that follows β 8. This helix extends from the body of the structure and mediates a domain swap through which β -strands β 9 and β 10 complete the β -sheet fold of the other member of the dimer (Fig. 1e).

The domain swapped β 9- β 10 element comprising Gln152-Lys164 makes extensive interactions with the SARAF_L core that are mediated by the formation of anti-parallel β -sheet main chain hydrogen bonds between β 9- β 5 and a short parallel β -sheet made between β 10 and β 6 and that bury 2232 Å² per tail-body interface. (Fig.1c-e). The backbone β -sheet interactions are accompanied by a number of sidechain mediated interactions. Cross-strand hydrogen bonds are formed by His153-Tyr105 (Fig. S1c), a network comprising Ser157, Ser159, and Thr110 (Fig. S1d), and a Tyr163 hydroxyl and Tyr91 carbonyl interaction (Fig. 1e). Phe155 and Phe158 sidechains rest in shallow grooves on the surface the SARAF_L core while the Tyr161 sidechain is buried in a largely hydrophobic pocket (Fig. 1e). Finally, the Lys164 C-terminal carboxylate forms a hydrogen bond to the amide of Gly116 and salt-bridge with the Arg57 sidechain (Fig. 1e). Despite being involved in a Ca²⁺-dependent process, SARAF lacks any obvious Ca²⁺-binding motifs [24]. Examination of the surface electrostatic potential (Fig. 2) revealed a few disperse regions of negative potential, but none that would indicate a site for Ca²⁺-binding, as well as a large positive patch in a pocket near SS3. In accordance with this lack of clear Ca²⁺-binding motifs, even though the structure was determined in the presence of 1 mM CaCl₂, we found no crystallographic evidence for Ca²⁺ binding to SARAF_L.

Searches for structural homology between SARAF_L and proteins of known structure using the DALI database [28] revealed no strong matches, indicating that SARAF_L has a unique fold. Relaxation of the similarity criteria to allow for a generous Z-score cutoff (>2) identified a set of β -sheet structures that include the γ -COPI appendage domain (1R4X), Xenavidin (2UYW), Avidin-related protein 2 (1WBI), and a conserved domain from *Bacillus anthracis* (3FBQ) (Z-scores of 2.3, 2.2, 2.1 and 2.0 respectively)(Fig. 3). However, strand connectivity analysis reveals that SARAF_L is substantially different from each of these folds. Namely, SARAF_L lacks the Greek-key motif of Xenavidin and Avidin related protein 2, and is not composed of strictly anti-parallel β -sheets as are the γ -COPI appendage domain and the *Bacillus anthracis* conserved domain. Hence, SARAF_L has a novel β -sandwich architecture that we now call the SARAF-fold.

Analysis of >90 SARAF_L-related sequences uncovers a set of related proteins spanning all five vertebrate classes (mammals, birds, amphibians, fish and reptiles), including some very ancient animals such as the sea lamprey (*Petromyzon marinus*) and coelacanth (*Latimeria chalumnae*). This family of SARAF_L homologs all have strong conservation of the six cysteines that form the three SARAF_L disulfides as well as high conservation of many residues that form the core of the SARAF_L fold (Figs. 1b, 4a, and S2). We did not find SARAF-like sequences among other metazoans, but, surprisingly, identified a group of transmembrane proteins similar to SARAF_L in fungi, including organisms that are pathogens

of mammals, insects, or plants (Fig. S3). This group of SARAF_L homologs diverges more from human SARAF_L than the vertebrate sequences. For example, the exposed disulfide, SS1, lacks one of the cysteines in a small subset of the fungal sequences and the swapped β 9/ β 10 strand is not well conserved. Nevertheless, the data clearly identify the presence of key elements of the core SARAF_L structure (Fig. 4b). The unique nature of the SARAF_L structure, together with the presence of clear homologs in vertebrates and fungi indicates that SARAF_L structure represents a previously unknown, widely-occurring protein fold.

SARAF_L dimerization depends on the swapped domain

The presence of the domain-swapped dimer in the crystals prompted us to investigate the nature of this interaction further. Characterization by size exclusion chromatography and multi-angle light scattering (SEC-MALS) [29] indicated the dominant presence of SARAF_L monomers in solution at 64 μ M (observed 15.84 ± 0.08 kDa, calculated 15.49 kDa) (Fig. 5a). Further probing with glutaraldehyde crosslinking revealed a dimeric species that appeared with increasing protein concentrations into the 100 μ M range (Fig. 5b), suggesting that the propensity to dimerize is weak. As the domain swapped dimer observed requires an exchange of β 9 and β 10 (Fig. 1c and d), we created a SARAF_L deletion construct truncated at residue 150 to remove the domain-swapped β -strands β 9 and β 10 (β 9/ β 10). Expression and purification of SARAF_L(β 9/ β 10) yielded a protein having similar properties to SARAF_L running as a monomer on gel filtration (Fig. S4a and b) and having a similar circular dichroism spectrum to SARAF_L, indicative of a folded protein (Fig. S4c). Notably, the deletion of the domain-swapped strands, β 9 and β 10, dramatically diminished the ability of the protein to be crosslinked by glutaraldehyde (Fig. 5b), supporting the idea that the dimer seen in SARAF_L relies on the domain swap interaction of β 9 and β 10. To probe the strength of SARAF_L dimer formation, we used equilibrium analytical ultracentrifugation. Fits of the SARAF_L data using a single species monomer model yielded upwardly curving residuals, particularly at the highest concentration (200 μ M), that were indicative of a poor fit and the formation of a higher-order species (Fig. S4d). Accordingly, the SARAF_L data could be well fit with a monomer-dimer association model (Fig. 5c and d), as indicated by the uniformly stochastic residuals. This analysis yields an estimate of the SARAF_L dissociation constant in the low millimolar range ($K_d \sim 2$ mM). Such a value is entirely in line with the observation that SARAF_L is monomeric under the low micromolar concentrations conditions used for SEC-MALS (Fig. 4a). In contrast to the behavior of SARAF_L, equilibrium analytical sedimentation studies of SARAF_L(β 9/ β 10), which lacks the ability to form domain-swapped dimers, showed that this construct behaved as a monomeric protein that was well fit by a single species model (Fig. 5e). Together with the crosslinking studies, these data demonstrate that the domain swap of the SARAF_L β 9/ β 10 element is essential for dimerization.

SARAF self-associates in the ER

Given that purified SARAF_L forms dimers in solution, we sought to probe the extent to which such an interaction might occur in the context of a cell. We transfected HEK293 cells with equal amounts of full-length SARAF constructs bearing the fluorescent proteins, green fluorescent protein (GFP) [30] or mCherry [31], fused to the SARAF N-terminus (GFP-SARAF and mCherry-SARAF) and measured the Förster Resonance Energy Transfer

(FRET) between the two constructs. We determined the amount of FRET by measuring the fluorescence emitted from mCherry under exclusive excitation of GFP, using Dual-View imaging, and quantified as the ratio of the red to green fluorescent intensities (FRET signal) (Fig 4f). We then used a similar approach with N-terminally-tagged soluble luminal domains SARAF(165–339) that lacked the transmembrane anchor and that were targeted to the ER lumen by bearing both the SARAF signal peptide (SP) and a C-terminal retention signal (KDEL). FRET signals from the GFP-SARAF(165–339) and mCherry-SARAF(165–339) pair were substantially smaller than the GFP-SARAF and mCherry-SARAF pair but were still well above background (Fig. 5g). These results suggest that, in line with the biochemical studies, the SARAF luminal domains self-associate in the ER. This association happens whether the luminal domain is soluble form confined to the ER or is membrane anchored. The stronger FRET signals from the full-length constructs indicate that membrane anchoring enhances the luminal domain effective concentration [32, 33] and facilitates self-association.

Because of the domain swapped SARAF_L dimer architecture, there is a much shorter distance between the N-termini and C-termini of the dimer partners (19.6 Å, C α -C α) than between the N- and C- termini of an individual subunit (66.7Å, C α -C α) or the N- and C-termini of the dimer partners (75.4 Å and 61.8 Å, respectively) (Fig. S4e). These constraints predict that FRET signals will be larger between constructs in which the fluorophores are placed on opposite termini of the tested pairs (i.e. N-donor and C-acceptor). In line with this prediction, FRET between the GFP-SARAF_L:SARAF_L-mCherry pair was ~3-fold larger than the FRET signals observed from co-expressed pairs having each fluorophore fused to the SARAF_L N-terminus, GFP-SARAF and mCherry-SARAF (Fig. 5h). Furthermore, in both cases, co-expression of untagged SARAF(165–339) reduced the FRET signals to background levels, indicating that the FRET signals derive from co- association of the test proteins (Fig. 5i). Together, these data strongly support the notion that the domain swapped form of the SARAF_L occurs in a cellular context, forms in the full-length protein in cell membranes, that similar to in solution, self-association is reversible.

Design and characterization of SARAF_L ‘Cys-lock’ mutants identifies the SARAF luminal switch domain

The crosslinking and sedimentation equilibrium studies suggest that domain-swapped dimer exchanges freely with the monomeric state. In order to characterize properties of the monomer and dimer forms separately, we set out to create a SARAF_L mutant that would be incapable of domain swap. We reasoned that incorporation of a fourth disulfide bond between the swapped strand and the core of SARAF_L structure could serve as a ‘Cys-lock’ that would covalently tether the swapped β 9/ β 10 strand to the body of the protein. We identified a residue pair, Lys98-Ala156 on strands β 6 and β 9, as having favorable geometry to form such a disulfide when each member was mutated to cysteine. Purification of SARAF_L K98C/A156C by ion exchange chromatography revealed the presence of two species corresponding to monomer and dimer forms present in a ratio of ~10:1 (Fig. S4f) and having different mobilities on size exclusion chromatography (Fig. 6a). SDS-PAGE under non-reducing conditions revealed two, separate species that ran at molecular weights consistent with the monomeric form (15.5 kDa) and the dimeric form (31.0 kDa). By

contrast, both species ran identically upon addition of reducing agent (Fig. 6b), indicating that the two forms are the disulfide linked dimer (16.5 ml form) and disulfide linked monomer (18.3 ml form), respectively (Fig. 6a). Both SARAF_L K98C/A156C forms produced crystals that diffracted X-rays to high resolution, 1.58Å and 2.1Å for the monomer and dimer, respectively (Table S1). Molecular replacement using the SARAF_L core lacking the surface loops and the β 9/β10 strand, revealed clear electron density in both structures for the engineered K98C/A156C ‘Cys-lock’ disulfide (Fig. 6c and d). Model building and refinement revealed that the Cys-lock monomer and Cys-lock dimer protomer maintain the same overall fold as the wild-type SARAF_L dimer protomer (Fig. 6e) (RMSD_{Cα} = 0.739 and 0.590 for residues 33–145 of the Cys-lock monomer and Cys-lock dimer versus SARAF_L, respectively). Notably, the SARAF_L K98C/A156C Cys-lock monomer has the marked difference that the tail, which extends from the core in the dimeric form, is wrapped under the bottom of SARAF_L so that β 9/β 10 inserts in *cis* to complete the anti-parallel and mixed β -sheets of the SARAF_L fold (Fig. 6d). The α₁ helix is retained despite this topology change of the SARAF_L tail, although it shorter by one helical turn relative to the dimer form. In both the Cys-locked dimer and the Cys-locked monomer the electrostatic surface potentials were very similar to wild-type SARAF_L (Fig. S5). These structural studies demonstrate that the switch from monomer to dimer requires changes only in the β 9/β 10 tail and not the SARAF_L core. Accordingly, we term the β 9/β 10 tail as the ‘SARAF luminal switch domain’.

SARAF dimerization affects SOCE inactivation

To test the functional importance of the SARAF luminal switch, we used whole-cell patch clamp to measure SOCE currents from HEK293 cells that were co-transfected with Orai1-CFP and STIM1-mCherry along with GFP tagged version of SARAF, SARAF-GFP, or a SARAF mutant lacking the luminal switch, SARAF (β 9/β 10)-GFP. Recording conditions included 1,4-Dihydroxy-2,5-di-*tert*-butylbenzene, (BHQ), a reversible SERCA inhibitor, to allow for both depletion and refilling of Ca²⁺ stores. Because we observed a direct relationship between STIM1 expression level and Orai1 current density (Fig. S6), we limited our analysis to cells expressing STIM1-mCherry at or below a threshold of 5000 fluorescence counts/cell to ensure that any functional effects were not due to exceptionally high levels of STIM1. Cells expressing SARAF-GFP or SARAF(β 9/β10)-GFP had comparable levels of STIM1 expression (Fig. 7a and b) and similar passive membrane properties. However, we observed that the SOCE current densities 18s after addition of external Ca²⁺ to activate the current were roughly twice as large in cells expressing SARAF(β 9/β 10)-GFP versus SARAF-GFP (42.6±7.5 pA/pF (n=9) and 21.2±4.3 pA/pF (n=11) p<0.05, respectively) (Fig.6c). Further, the time to maximum response for SOCE current activation was faster by ~2-fold in cells expressing the SARAF luminal switch mutant (17.1±1.7s and 32.5±4.6s (n=11) and (n=9), p<0.01, for SARAF (β 9/β10)-GFP and SARAF-GFP, respectively) (Fig. 7d). These results indicate that the self-associated form of SARAF accelerates SOCE inactivation and that domain swap of the luminal switch is important for stabilizing this state.

Discussion

SARAF is a transmembrane, ER-resident, negative regulator of SOCE [24]. Understanding how it influences SOCE has been limited due to its lack of similarity to proteins of known structure. Crystallographic determination of the structure of the SARAF luminal domain, SARAF_L, shows that this domain comprises a novel, ten-strand β -sheet fold constrained by three conserved disulfides that we name the ‘SARAF-fold’. Although, the SARAF fold belongs to a class of β -sheet sandwich proteins represented by the γ -COPI appendage domain (1R4X), Xenavidin (2UYW), Avidin-related protein 2 (1WBI), and a *Bacillus anthracis* conserved domain (3FBQ) (Fig. 3), the SARAF fold and topology are unique. Homologs having all six cysteines that form the three SARAF_L disulfides as well as many conserved core residues in the SARAF_L core occur in all five vertebrate classes (mammals, birds, amphibians, fish and reptiles), including quite ancient members of this phylum, such as the sea lamprey (*Petromyzon marinus*) and coelacanth (*Latimeria chalumnae*) (Figs. 1b, 4a and S2). Although SARAF_L is widespread among vertebrates, it appears to be absent from other metazoans. Intriguingly, we found a set of fungal transmembrane proteins that are also SARAF_L homologs (Figs. 4b and S3). This unusual distribution of homologs in both vertebrates and fungi establishes that the previously unknown SARAF-fold is widespread. Because fungi are not known to use the SOCE pathway, it seems likely that the SARAF-fold has other functions beyond its role in SOCE regulation.

Apart from its unique fold, our structural studies revealed a second key feature of the SARAF_L fold, the ability to domain-swap. The formation of intertwined protein assemblies by exchange of identical structural elements is observed in many classes of soluble and transmembrane proteins [34–37]. Although this phenomenon provides a straightforward mechanism for homo-oligomer formation, its functional relevance is often not clear [34, 37, 38]. In SARAF_L, the swapped domain is a simple element comprising the β 9 and β 10 β -strands that insert into the essentially rigid, stable core of the rest of the fold.

Two structure-based protein design strategies firmly establish that the β 9/ β 10 strands form the dimerization element. First, design of SARAF_L mutant lacking β 9 and β 10 yielded a well-folded, stable protein that only differed from SARAF_L in its inability to dimerize. Second, structure-based design to incorporate a disulfide between β 9 and the SARAF_L core yielded two covalently trapped species, a covalent dimer and a self-ligated monomer. Structural studies show that apart from the topological change, these two forms are identical. The intrinsic affinity of SARAF luminal switch mediated dimerization is modest having a dissociation constant in the low millimolar range ($K_d \sim 2$ mM). Nevertheless, the transmembrane nature of full-length SARAF clearly imposes diffusional restrictions that serve to increase the effective concentration [32, 33] and favor self-association (Fig. 5g). Importantly, overexpression of non-membrane anchored SARAF_L is able to suppress the amount of dimer, indicating that full-length SARAF self-association is reversible (Fig. 5h). Hence, we term the β 9/ β 10 element as the ‘SARAF luminal switch’ domain, as biochemically this is the sole element required to convert between monomeric and dimeric forms and this domain is necessary for self-association of SARAF in membranes.

A hallmark of the SOCE pathway is that it is governed by reversible self-association of the ER sensor, STIM, in response to changes in ER calcium levels [15, 17–22]. SARAF functional studies indicate that domain-swap mediated self-association is key for the ability of SARAF to accelerate inactivation of the SOCE current (Fig. 7). Whether, as with STIM1, SARAF also forms higher order oligomers remains to be elucidated. In this regard, it is worth noting that crystal packing of SARAF_L shows a simple face-to-face arrangement in which the C-termini that link SARAF_L to the transmembrane portion all face the same direction (Fig. S1b). Such an arrangement would be compatible with formation of higher order assemblies of SARAF dimers in the context of the membrane. Nevertheless, even though the self-associated form of SARAF_L is a dimer in both the crystal structure and in solution, non-symmetric domain swapping via the SARAF luminal switch could also form higher-order domain swapped assemblies as has been observed in other domain-swapped proteins [38]. Hence, even though SARAF clearly self-associates in the membrane (Fig. 5g–i), and this association is important for function, the stoichiometry of self-organization and how such assemblies might be affected by interactions with STIM or Orai requires further investigation.

Initial characterization of SARAF demonstrated that it acts in a calcium-dependent manner, inhibiting SOCE only when ER stores were refilled with calcium [24]. SARAF_L has no identifiable Ca²⁺-binding motifs and despite being crystallized in 1 mM CaCl₂, there is no evidence for non-canonical binding sites for Ca²⁺ on SARAF_L. Hence, how SARAF senses and responds to ER Ca²⁺ changes remains to be discovered. Given the absence of Ca²⁺ binding to SARAF_L, it may be that there is some type of Ca²⁺-mediated interaction of SARAF_L with the membrane inner leaflet or Ca²⁺-dependent control of SARAF by a yet to be defined ER Ca²⁺-sensor protein.

SOCE is a complex, multicomponent process that involves the reversible, coordinated association of proteins in both the ER and plasma membranes [15]. The ER resident transmembrane protein SARAF serves an important role in this phenomenon by fine-tuning SOCE activity in response to ER refilling with Ca²⁺. The discovery that the SARAF luminal domain has a unique, disulfide-bonded β-sheet protein fold, capable of domain-swap mediated self-assembly that impacts function sets a key structural framework for understanding the basic roles of SARAF in controlling SOCE and the possible roles for SARAF in cancer, neurodegenerative diseases, and cardiomyopathy [39–43].

Materials and Methods

Protein expression and purification

Human SARAF_L (residues 30–164) or SARAF_L((β9/(β10) (residues 30–150) were cloned into a modified version of the pET28 vector containing an N-terminal combination His₆ and Maltose Binding protein tag followed by TEV protease site (HMT). Point mutants were introduced using site directed mutagenesis. The SARAF_L or SARAF_L((β9/(β10) constructs were transformed into SHuffle Express cells (NEB) and grown in 1L cultures of 2YT media at 37°C. The SHuffle Express cells have deletions of the genes for glutaredoxin reductase and thioredoxin reductase (*gor* *trxB*), which allow disulfide bonds to form in the cytoplasm. Additionally, they constitutively express a chromosomal copy of the disulfide

bond isomerase DsbC allowing for rearrangement of improperly oxidized disulfides. Cultures were induced with 0.5 mM IPTG at an OD_{600nm} of ~0.6 and moved to 24°C. Protein was expressed overnight and cells were harvested by centrifugation and then immediately flash frozen in liquid nitrogen and stored at -80°C. Frozen cell pellets were thawed on ice and resuspended in lysis buffer (25 mM HEPES pH 7.4, 300 mM KCl, 1 mM CaCl₂, 10 mM Imidazole, 1 mM PMSF, 1 μg ml⁻¹ DNaseI) at a ratio 6 ml lysis buffer to 1g cell pellet. Resuspended cells were disrupted by sonication and insoluble material pelleted by centrifugation. Clarified lysate was mixed with 2 ml bed volume of Talon beads (Clonotech) and incubated while rocking for 1 hour at 4°C. Following incubation, beads and lysate were transferred to a gravity flow column at washed with 2 × 30ml lysis buffer before eluting with 15 ml lysis buffer containing 400 mM imidazole. After elution, protein was digested overnight with TEV at 4°C and buffer exchanged into 10 mM Tris, pH 8.8, 10 mM KCl over a HiPrep desalting column. Desalted SARAF was then passed over a POROS MC20 column followed by an Amylose column to remove TEV and cleaved MBP. SARAF was further purified by MonoQ ion exchange before final gel filtration in 10 mM HEPES, pH7.4, 200 mM KCl, 1 mM CaCl₂ and concentrated to 10 mg ml⁻¹ for crystallization.

The double mutant SARAF_L K98C/A156C was expressed and purified following the same protocol as wild type protein with the separation of monomer and dimer populations occurring at the ion exchange step before proceeding on to gel filtration. SARAF 31–164 K98C/A156C monomer and dimer were concentrated to 10 mg ml⁻¹ and 4mg ml⁻¹ respectively prior to crystallization.

Crystallization and Data Collection

Crystals used for structure determination of the wild type construct were grown in 0.1 M BisTris, pH 6.5, 18–20% PEG 5000 MME in hanging drop format. Crystallization drops were set over a thin layer of vacuum grease to prevent crystals from sticking to the cover slips and facilitate harvesting. Harvested crystals were cryoprotected by sequential soaks in mother liquor plus 5%, 10%, 15% and 20% glycerol before flash cooling in liquid nitrogen. For experimental phasing, crystals were soaked with 1 mM K₂Pt(NO₂)₄ overnight before back-soaking into mother liquor and cryoprotecting in glycerol as above. Crystals of SARAF 30–164 K98C/A156C monomer were grown in 0.1 M sodium acetate, pH 4.2–4.6 and 1.2–1.6 M sodium formate in standard hanging drop format without the use of vacuum grease. Harvested crystals were cryoprotected by sequential soaks in mother liquor plus 5%, 10%, 15% and 20% glycerol before flash cooling in liquid nitrogen. Crystals of SARAF 30–164 K98C/A156C dimer were grown in 3–5% glycerol or ethylene glycol after first treating protein to mild heating at 37°C for 5 minutes or ultracentrifugation (40000 rpm, 30min, 4°C) to remove microcrystals that spontaneously form in concentrated protein solution. Harvested crystals were cryoprotected by directly soaking in 25% ethylene glycol before flash cooling in liquid nitrogen

Data were collected at Advanced Light Source beamline 8.3.1. Native datasets of wild type SARAF were collected at a wavelength of 1.127Å and diffracted to 1.90Å. Peak, inflection and high remote datasets were collected from K₂Pt(NO₂)₄-soaked crystals and diffracted to a resolution of 2.15Å. Native datasets for both SARAF K98C/A156C monomer and dimer

were collected at a wavelength of 1.116Å and diffracted to resolutions of 1.58Å and 2.10Å respectively.

Data Processing and Structure Determination

Data from both native and K₂Pt(NO₂)₄-soaked wild type crystals were indexed, integrated, and scaled in spacegroup C2 using autoPROC [44]. autoSHARP [45] was used to determine initial experimental phases using peak, inflection, and remote datasets from K₂Pt(NO₂)₄-soaked crystals finding a total of 10 platinum sites. An initial model was obtained using ARP/wARP [46] and improved with iterative rounds of manual rebuilding with COOT [47] and refinement with Phenix [48]. The SARAF K98C/A156C monomer and dimer structures were phased by molecular replacement with PHASER [49] using the wild type structure with the tail and surface loops removed as a search model. As with the wild type structure, the models were improved with iterative rounds of manual rebuilding in COOT [47] and refinement in Phenix [48].

Analytical Ultracentrifugation

Sedimentation equilibrium experiments were performed at 4°C in an Optima XL-I analytical ultracentrifuge (Beckman Coulter). Prior to loading the rotor cells, 500 µl of SARAF_L or SARAF_L((β 10) was dialyzed against 1 L of buffer (200 mM KCl, 10 mM HEPES, pH 7.4) overnight at 4°C. 125 µl of SARAF_L or SARAF_L((β 9/(β 10) were loaded into six chamber center pieces at three concentrations of 20 µM, 60 µM and 200 µM determined by absorbance at 280 nm [50]. 115 µl of dialysate buffer was loaded into adjacent reference chambers. Data were acquired using interference optics at rotor speeds of 10K, 18K, 22K and 31K rpm. Data acquired at multiple loading concentrations and rotor speeds were modeled globally in IgorPro using a standard monomer-dimer self-association model. V_{bar} and solvent density were calculated using Sednterp and the interference extinction coefficient was calculated using the formula $e_{\text{int}} = 2.733 * MW$. For global fitting, V_{bar} , MW, solvent density and e_{int} were held constant while K_d (for N = 2) was allowed to float.

Glutaraldehyde crosslinking

Purified SARAF_L or SARAF_L((β 9/(β 10) in a buffer of 10 mM HEPES, pH 7.4, 200 mM KCl at concentrations ranging from 25 µM to 100 µM, determined by absorbance at 280 nm [50] were combined with 0.01% glutaraldehyde (Aldrich) in a final volume of 10 µl and incubated at room temperature for 10 minutes. Reactions were quenched by adding 1 µl of 1 M Tris pH 8.0 to achieve a final concentration of 100 mM, Tris pH 8 and were then boiled for 10 min in reducing SDS-sample buffer prior. Samples were subsequently analyzed by SDS-PAGE.

SEC-MALS

Multi-angle light scattering (MALS) experiments were carried out at 4°C using an HPLC (Shimadzu) with UV detector connected to a miniDAWN TREOS MALS detector and an Optilab T-rEX refractometer (Wyatt Technology). 100 µl of 1mg ml⁻¹ of purified SARAF_L was injected onto a Superdex S200 10/300 GL column (GE Healthcare) equilibrated in 200 mM KCl, 10 mM HEPES, pH7.4, and eluted peak was detected online. Molecular weight

was calculated at each time point during elution using a combination of UV absorbance, light scattering and differential refractive index measurements with the Astra software package (Astra 6.0, Wyatt Technology). The experimentally determined molecular weight of SARAF_L of 15.84 kDa (+/- 0.509%) compares well with the 15.49kDa calculated from the protein sequence. SARAF_L was monodisperse with a polydispersity ratio (Mw/Mn) of 1.000 (+/- 0.719%).

Circular Dichroism

Prior to measurement, 600 µl each of 10 µM SARAF_L and 10 µM SARAF_L ((β 9/(β 10), determined by absorbance at 280 nm [50], were dialyzed overnight at 4°C against 1 L of 30 mM sodium phosphate buffer. Circular dichroism spectra were measured with a 1 mm path length quartz cuvette using an Aviv model 215 spectropolarimeter (Aviv Biomedical) equipped with a Peltier temperature controller. Wavelength scans from 320 to 185 nm were taken at 1 nm intervals at 4°C. Each scan was performed in triplicate from the same sample and subtracted by the average of a triplicate scan of the dialysate for a matched buffer blank. Molar ellipticity was calculated as follows: $\theta = 100(m)/(Cnl)$, where m is the CD signal in millidegrees after buffer subtraction, C is the millimolar peptide concentration, n is the number of residues in the peptide, and l is the cuvette path length in centimeters.

Cell Culture

HEK293 cells were grown in DMEM supplied with fresh L-glutamine, sodium pyruvate, FBS and penicillin/streptomycin. Cells were split to 35mm plates one day prior to transfection. Transfection with 600 ng of C-terminally GFP-tagged SARAF or SARAF((β 9/(β 10), 200 ng of C-terminally mCherry- tagged STIM1 and 200 ng of C-terminally CFP-tagged Orai1 with PEI_{max} reagent (Polysciences) was performed 22–36 hours prior to imaging and electrophysiological experiments. Cells were transferred to poly-L-lysine covered 24 mm cover slips one night prior to the experiments.

Forster Resonance Energy Transfer

Cells were excited with 470/40 nm light for FRET measurements, fluorescent signals were collected through the objective and split using Dual-View device (565LP dichroic) to GFP (525/50) and mCherry (650/75) channels using EMCCD 512×512 (Princeton Instruments). Images were processed using SlideBook (Intelligent Imaging Innovations) software and exported as Microsoft Excel files. FRET signals were assessed by dividing the FRET (mCherry) channel by the GFP channel. GFP or mCherry were fused to the N-termini of SARAF_L (XFP-SARAF_L) or SARAF full length (XFP-SARAF) using the following sequence, SARAF(M1-G30)-TG-XFP-RT-SARAF(W31-K164)-KDEL or SARAF(M1-G30)-TG-XFP-RT-SARAF(W31-R339), respectively. Fusions of monomeric forms of GFP [30] or mCherry [31] were made at the end of the luminal domain (K164) of the SARAF_L (SARAF_L- XFP) or full length SARAF were at position K164 using the following sequence SARAF(1–164)-TG RPACKIPNDLKQKVMNH-XFP- KDEL or SARAF(M1-K164)-TGLGGGGSGGGSGGGGSAAARPACKIPNDLKQKVMNH-XFP-LGGGGSGGGSGGGGSAAASGLRS-SARAF(M173-R339), respectively. ER retention signal (KDEL) was added at the C-termini of all luminal SARAF constructs.

Electrophysiological recordings

Membrane currents were recorded under voltage-clamp conditions using the whole-cell patch-clamp configuration using an Axopatch 200B (Axon Instruments) amplifier. Patch pipettes were fabricated from borosilicate glass capillaries (2–5 M Ω). Signals were analog filtered using a 2 kHz low-pass Bessel filter. Data acquisition and analysis were done using pCLAMP 9 software (Molecular Devices). Current densities were calculated by normalizing currents to cell capacitance. The recording protocol consisted of a 60 ms hyperpolarizing step to –100 mV from 0 mV, followed by a 20 ms step to 0 mV, and a 120 ms ramp from –100 mV to +100 mV repeated at 0.5 Hz for 300s. All data were leak-corrected using the current in lanthanum-containing solution. The EGTA (ethylene glycol-bis(β - aminoethyl ether)-N,N,N',N'-tetraacetic acid) internal solution contained 150 mM Cs aspartate, 8 mM MgCl₂, 1.2 mM EGTA, 10 mM HEPES and 2 mM Mg-ATP. The pH was titrated to pH 7.2 with CsOH.

The external solution contained 145 mM NaCl, 2 mM MgCl₂, 2.8 mM KCl, 10 mM CsCl, 10 mM HEPES and 10 mM Glucose. The pH of the external solution was titrated to pH7.4 with NaOH. 10 mM CaCl₂, 100 μ M EDTA (ethylenediaminetetraacetic acid) or 10 mM MgCl₂, 1 mM EDTA were added to the external solution for high-Ca²⁺ or Ca-free solution, respectively. Fluorescence was measured from images acquired using EMCCD 1024 \times 1024 iXonUltra camera under epifluorescence, and analyzed with VisiView software (Visitron Systems GmbH). Cells were excited using Xcite Exacte (Excelitas technologies) using the following filters: excitation filters ET470/40 for GFP and FF01–580/14 for mCherry, emitted light was filtered with BP536/40 for GFP and HQ650/75 for mCherry. Data are presented as mean \pm S.E.M.

Supplementary Material

Refer to Web version on PubMed Central for supplementary material.

Acknowledgements

This work was supported by grants NIH-NHLBI R01-HL080050 and NIH-NIDCD R01-DC007664 to D.L.M., Israeli Science Foundation grant 1248/15 to E.R. US-Israel Binational Science Foundation 2015298 to D.L.M. and E.R. AHA 14POST18740062 and NIH-HLBI T32HL007731 to C.K., and an Israeli Ministry of Aliyah and Integration fellowship to A.M. E.R. is the incumbent of the Charles H. Hollenberg Professorial Chair.

References

- [1]. Clapham DE. Calcium signaling. *Cell*. 2007;131:1047–58. [PubMed: 18083096]
- [2]. Hille B *Ion Channels of Excitable Membranes*. 3rd ed. Sunderland, MA: Sinauer Associates, Inc.; 2001.
- [3]. Berridge MJ, Bootman MD, Roderick HL. Calcium signalling: dynamics, homeostasis and remodelling. *Nature Rev Mol Cell Biol*. 2003;4:517–29. [PubMed: 12838335]
- [4]. Carafoli E, Santella L, Branca D, Brini M. Generation, control, and processing of cellular calcium signals. *Critical reviews in biochemistry and molecular biology*. 2001;36:107–260. [PubMed: 11370791]
- [5]. Hodeify R, Yu F, Courjaret R, Nader N, Dib M, Sun L, et al. Regulation and Role of Store-Operated Ca(2+) Entry in Cellular Proliferation In: Kozak JA, Putney JW Jr., editors. *Calcium Entry Channels in Non-Excitable Cells*. Boca Raton (FL)2018 p. 215–40.

- [6]. Cahalan MD. STIMulating store-operated Ca(2+) entry. *Nat Cell Biol.* 2009;11:669–77. [PubMed: 19488056]
- [7]. Lewis RS. The molecular choreography of a store-operated calcium channel. *Nature.* 2007;446:284–7. [PubMed: 17361175]
- [8]. Putney JW Jr. A model for receptor-regulated calcium entry. *Cell calcium.* 1986;7:1–12. [PubMed: 2420465]
- [9]. Shim AH, Tirado-Lee L, Prakriya M. Structural and Functional Mechanisms of CRAC Channel Regulation. *Journal of molecular biology.* 2015;427:77–93. [PubMed: 25284754]
- [10]. Feske S A mutation in Orai1 causes immune deficiency by abrogating CRAC channel function. *Nature.* 2006;441:179–85. [PubMed: 16582901]
- [11]. Peinelt C Amplification of CRAC current by STIM1 and CRACM1 (Orai1). *Nature Cell Biol.* 2006;8:771–3. [PubMed: 16733527]
- [12]. Roos J STIM1, an essential and conserved component of store-operated Ca²⁺ channel function. *J Cell Biol.* 2005;169:435–45. [PubMed: 15866891]
- [13]. Soboloff J STIM2 is an inhibitor of STIM1-mediated store-operated Ca²⁺ entry. *Curr Biol.* 2006;16:1465–70. [PubMed: 16860747]
- [14]. Poteser M, Leitinger G, Pritz E, Platzer D, Frischauf I, Romanin C, et al. Live-cell imaging of ER- PM contact architecture by a novel TIRFM approach reveals extension of junctions in response to store-operated Ca(2+)-entry. *Sci Rep.* 2016;6:35656. [PubMed: 27759093]
- [15]. Prakriya M, Lewis RS. Store-Operated Calcium Channels. *Physiol Rev.* 2015;95:1383–436. [PubMed: 26400989]
- [16]. Qiu R, Lewis RS. Structural features of STIM and Orai underlying store-operated calcium entry. *Curr Opin Cell Biol.* 2019;57:90–8. [PubMed: 30716649]
- [17]. Bird GS, Hwang SY, Smyth JT, Fukushima M, Boyles RR, Putney JW Jr. STIM1 is a calcium sensor specialized for digital signaling. *Curr Biol.* 2009;19:1724–9. [PubMed: 19765994]
- [18]. Hogan PG, Lewis RS, Rao A. Molecular basis of calcium signaling in lymphocytes: STIM and ORAI. *Annu Rev Immunol.* 2010;28:491–533. [PubMed: 20307213]
- [19]. Kawasaki T, Lange I, Feske S. A minimal regulatory domain in the C terminus of STIM1 binds to and activates ORAI1 CRAC channels. *Biochem Biophys Res Commun.* 2009;385:49–54. [PubMed: 19433061]
- [20]. Lee KP. Molecular determinants of fast Ca²⁺-dependent inactivation and gating of the Orai channels. *Proc Natl Acad Sci USA.* 2009;106:14687–92. [PubMed: 19706554]
- [21]. Wu MM, Buchanan J, Luik RM, Lewis RS. Ca²⁺ store depletion causes STIM1 to accumulate in ER regions closely associated with the plasma membrane. *J Cell Biol.* 2006;174:803–13. [PubMed: 16966422]
- [22]. Zhou Y The short N-terminal domains of STIM1 and STIM2 control the activation kinetics of Orai1 channels. *J Biol Chem.* 2009;284:19164–8. [PubMed: 19487696]
- [23]. Parekh AB. Regulation of CRAC channels by Ca(2+)-dependent inactivation. *Cell calcium.* 2017;63:20–3. [PubMed: 28043696]
- [24]. Palty R, Raveh A, Kamisky I, Meller R, Reuveny E. SARAF inactivates the store operated calcium entry machinery to prevent excess calcium refilling. *Cell.* 2012;149:425–38. [PubMed: 22464749]
- [25]. Albarran L, Lopez JJ, Gomez LJ, Salido GM, Rosado JA. SARAF modulates TRPC1, but not TRPC6, channel function in a STIM1-independent manner. *Biochem J.* 2016;473:3581–95. [PubMed: 27506849]
- [26]. Jha A, Ahuja M, Malet J, Moreno CM, Yuan JP, Kim MS, et al. The STIM1 CTID domain determines access of SARAF to SOAR to regulate Orai1 channel function. *The Journal of cell biology.* 2013;202:71–9. [PubMed: 23816623]
- [27]. Zhang Z, Henzel WJ. Signal peptide prediction based on analysis of experimentally verified cleavage sites. *Protein science : a publication of the Protein Society.* 2004;13:2819–24. [PubMed: 15340161]
- [28]. Holm L, Rosenstrom P. Dali server: conservation mapping in 3D. *Nucleic acids research.* 2010;38:W545–9. [PubMed: 20457744]

- [29]. Foltá-Stogniew E Oligomeric states of proteins determined by size-exclusion chromatography coupled with light scattering, absorbance, and refractive index detectors. *Methods Mol Biol.* 2006;328:97–112. [PubMed: 16785643]
- [30]. Zacharias DA, Violin JD, Newton AC, Tsien RY. Partitioning of lipid-modified monomeric GFPs into membrane microdomains of live cells. *Science.* 2002;296:913–6. [PubMed: 11988576]
- [31]. Shaner NC, Campbell RE, Steinbach PA, Giepmans BN, Palmer AE, Tsien RY. Improved monomeric red, orange and yellow fluorescent proteins derived from *Discosoma* sp. red fluorescent protein. *Nature biotechnology.* 2004;22:1567–72.
- [32]. Jencks WP. *Catalysis in Chemistry and Enzymology.* Dover ed. New York, NY: Dover Publications; 1987.
- [33]. Creighton TE. *Proteins: Structures and Molecular Properties.* 2nd ed. New York: W.H. Freeman and Company; 1993.
- [34]. Wodak SJ, Malevanets A, MacKinnon SS. The Landscape of Intertwined Associations in Homooligomeric Proteins. *Biophysical journal.* 2015;109:1087–100. [PubMed: 26340815]
- [35]. Bennett MJ, Eisenberg D. The evolving role of 3D domain swapping in proteins. *Structure.* 2004;12:1339–41. [PubMed: 15296726]
- [36]. Bennett MJ, Choe S, Eisenberg D. Domain swapping: entangling alliances between proteins. *Proceedings of the National Academy of Sciences of the United States of America.* 1994;91:3127–31. [PubMed: 8159715]
- [37]. Rousseau F, Schymkowitz J, Itzhaki LS. Implications of 3D domain swapping for protein folding, misfolding and function. *Advances in experimental medicine and biology.* 2012;747:137–52. [PubMed: 22949116]
- [38]. Mackinnon SS, Malevanets A, Wodak SJ. Intertwined associations in structures of homooligomeric proteins. *Structure.* 2013;21:638–49. [PubMed: 23523426]
- [39]. Chen X, Long F, Cai B, Chen X, Chen G. A novel relationship for schizophrenia, bipolar and major depressive disorder Part 7: A hint from chromosome 7 high density association screen. *Behavioural brain research.* 2015;293:241–51. [PubMed: 26192912]
- [40]. Romanuik TL, Ueda T, Le N, Haile S, Yong TM, Thomson T, et al. Novel biomarkers for prostate cancer including noncoding transcripts. *Am J Pathol.* 2009;175:2264–76. [PubMed: 19893039]
- [41]. Romanuik TL, Wang G, Holt RA, Jones SJ, Marra MA, Sadar MD. Identification of novel androgen-responsive genes by sequencing of LongSAGE libraries. *BMC Genomics.* 2009;10:476. [PubMed: 19832994]
- [42]. Twine NA, Janitz K, Wilkins MR, Janitz M. Whole transcriptome sequencing reveals gene expression and splicing differences in brain regions affected by Alzheimer's disease. *PloS one.* 2011;6:e16266. [PubMed: 21283692]
- [43]. Camargo A, Azuaje F. Identification of dilated cardiomyopathy signature genes through gene expression and network data integration. *Genomics.* 2008;92:404–13. [PubMed: 18595652]
- [44]. Vonnrhein C, Flensburg C, Keller P, Sharff A, Smart O, Paciorek W, et al. Data processing and analysis with the autoPROC toolbox. *Acta Crystallogr D Biol Crystallogr.* 2011;67:293–302. [PubMed: 21460447]
- [45]. Vonnrhein C, Blanc E, Roversi P, Bricogne G. Automated structure solution with autoSHARP. *Methods in molecular biology.* 2007;364:215–30. [PubMed: 17172768]
- [46]. Langer G, Cohen SX, Lamzin VS, Perrakis A. Automated macromolecular model building for X-ray crystallography using ARP/wARP version 7. *Nat Protoc.* 2008;3:1171–9. [PubMed: 18600222]
- [47]. Emsley P, Lohkamp B, Scott WG, Cowtan K. Features and development of Coot. *Acta Crystallogr D Biol Crystallogr.* 2010;66:486–501. [PubMed: 20383002]
- [48]. Adams PD, Afonine PV, Bunkoczi G, Chen VB, Davis IW, Echols N, et al. PHENIX: a comprehensive Python-based system for macromolecular structure solution. *Acta Crystallogr D Biol Crystallogr.* 2010;66:213–21. [PubMed: 20124702]
- [49]. McCoy AJ, Grosse-Kunstleve RW, Adams PD, Winn MD, Storoni LC, Read RJ. Phaser crystallographic software. *J Appl Crystallogr.* 2007;40:658–74. [PubMed: 19461840]
- [50]. Edelhoch H Spectroscopic determination of tryptophan and tyrosine in proteins. *Biochemistry.* 1967;6:1948–54. [PubMed: 6049437]

Highlights

- SARAF luminal domain, SARAF_L is a novel, (β -sandwich fold
- SARAF_L associates as a domain-swapped dimer using the SARAF luminal switch segment
- Self-association of SARAF via the luminal switch accelerates SOCE inactivation

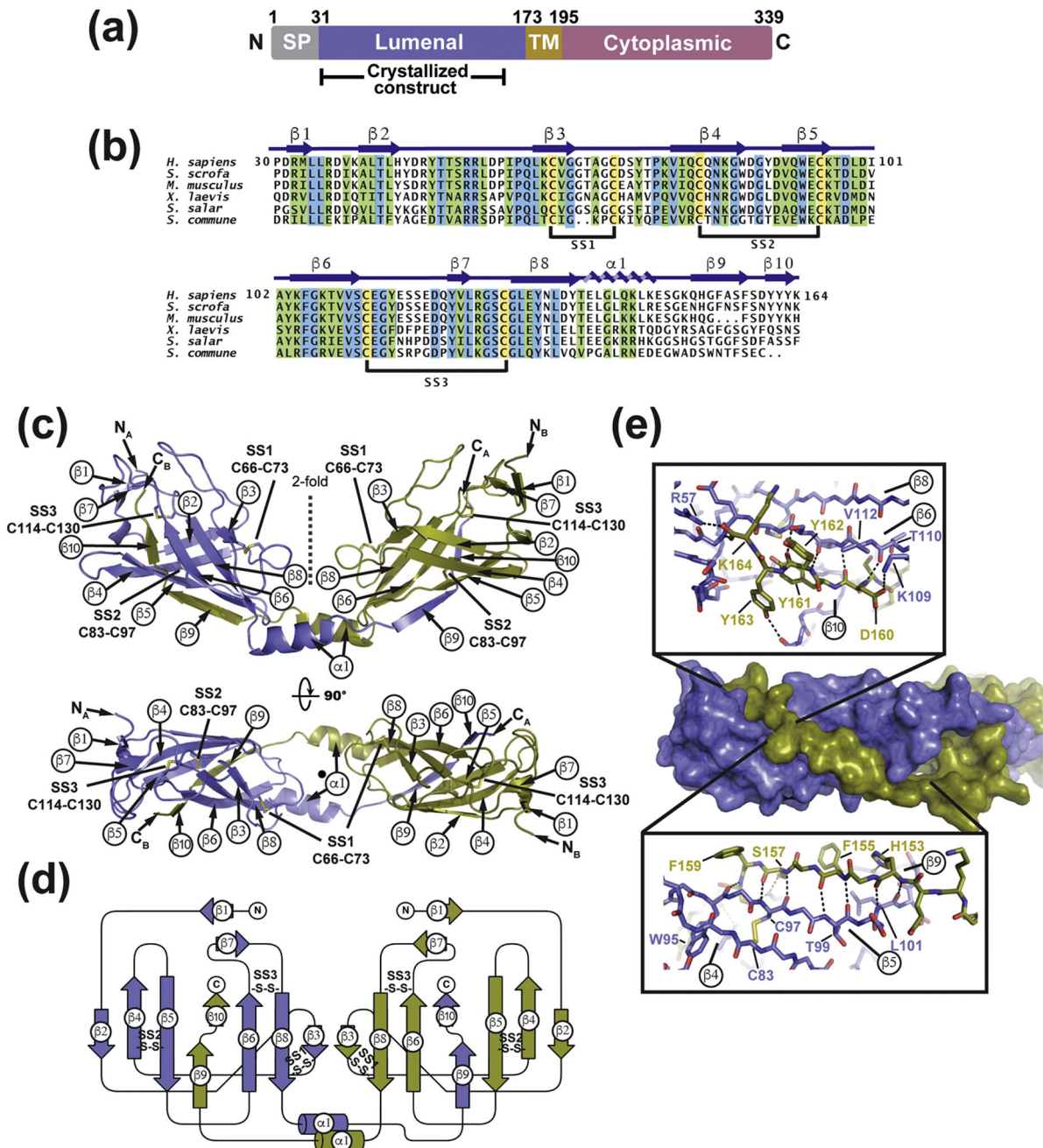


Fig. 1. Structure of SARAF_L

(a) SARAF schematic. Signal peptide (SP, grey), luminal (purple), transmembrane (TM, brown), and cytoplasmic (magenta) domains and amino acid boundaries of each are indicated. Extent of crystallized SARAF_L construct is shown. **(b)** SARAF_L sequence comparison from human (*H. sapiens*), pig (*S. scrofa*), mouse (*M. musculus*), frog (*X. laevis*), salmon (*S. salar*), and mushroom (*S. commune*). Invariant (blue), conserved (green) and cysteines (yellow) are highlighted. Secondary structure elements and disulfide bonds (SS1, SS2, and SS3) are shown. **(c)** Structure of the SARAF_L domain swapped dimer. N and C termini (N_A, N_B, C_A, and C_B) and secondary structure elements of each chain are labeled.

Disulfide bonds are shown as sticks and are labeled. Chains A and B are slate and deep olive, respectively. **(d)** SARAF_L domain swapped dimer topology diagram. 'S-S' denotes disulfide bonds. **(e)** Detailed view of interactions of domain swapped β 9 and β 10 with the SARAF_L core. Dashed lines indicate hydrogen bonds.

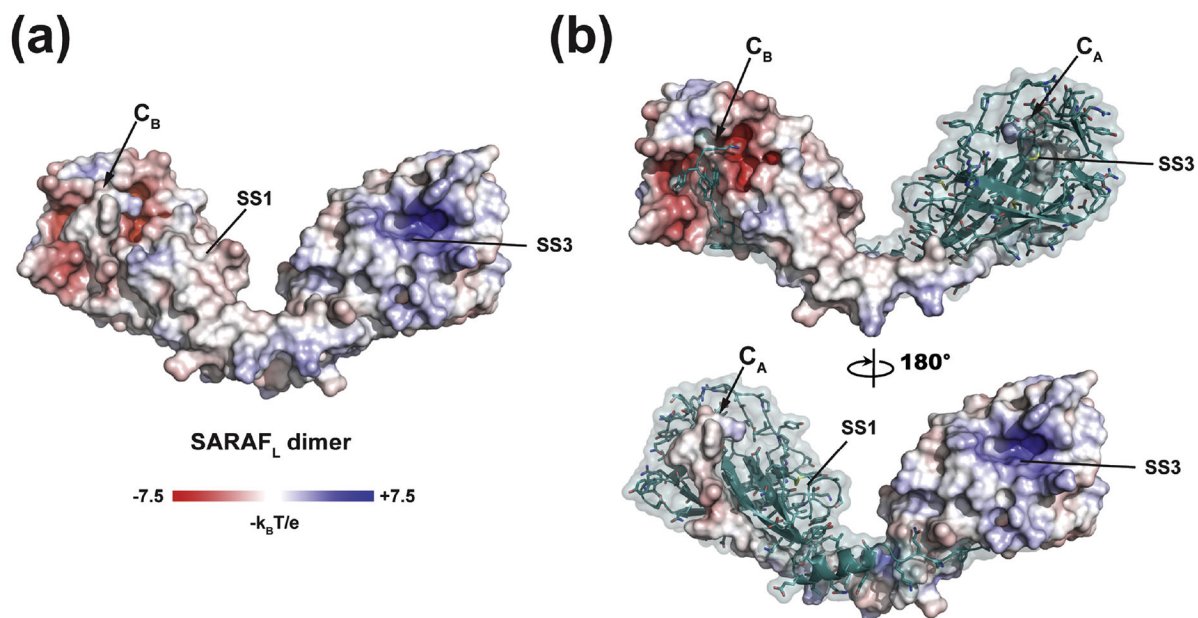


Fig. 2. SARAF_L electrostatic surface potential.

(a) Electrostatic surface potential for the SARAF_L dimer calculated in 150 mM ionic strength. **(a)** Electrostatic surface potential for one monomer of the SARAF_L dimer. In both panels, select elements are labeled.

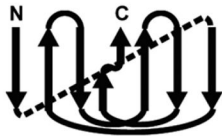
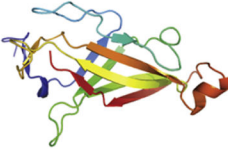

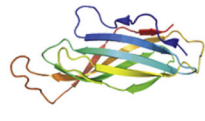
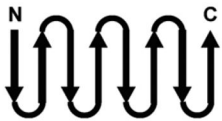
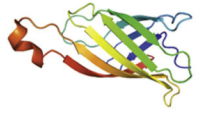

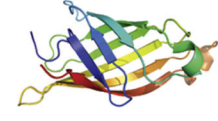

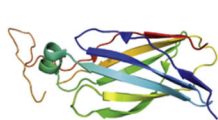
Protein (PDB)	Z-score	RMSD (Å)	Strand order	Structure
SARAF _L	—	—		
γ-COPI (1R4X)	2.3	2.9		
Xenavidin (2UYW)	2.2	4.1		
Avidin related protein 2 (1WBI)	2.1	4.1		
<i>Bacillus anthracis</i> conserved domain (3FBQ)	2.0	3.6		

Fig. 3. Analysis of the SARAF_L fold.

SARAF_L structural homologs identified using DALI [28]. DALI search Z-score, RMSD_{Ca}, diagram of strand topology, and structure are shown. Cartoon representations highlighting secondary structure elements are colored by rainbow from N-terminus (blue) to C-terminus (red).

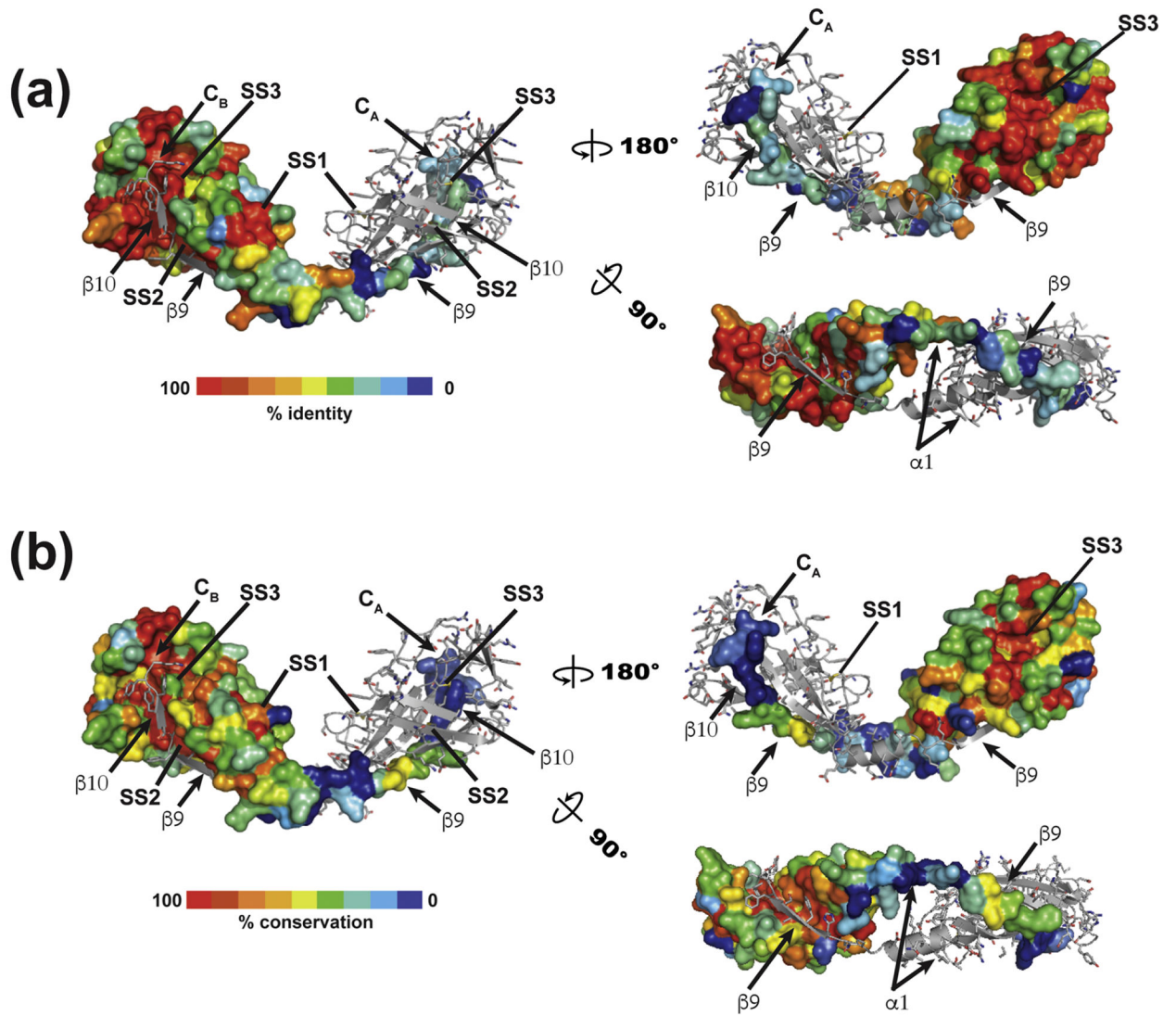


Fig. 4. Conservation mapping of vertebrate sequences on the SARAF_L structure for (a) vertebrate and (b) fungal sequences. One member of the dimer is shown in surface rendering. Select structural elements are labeled.

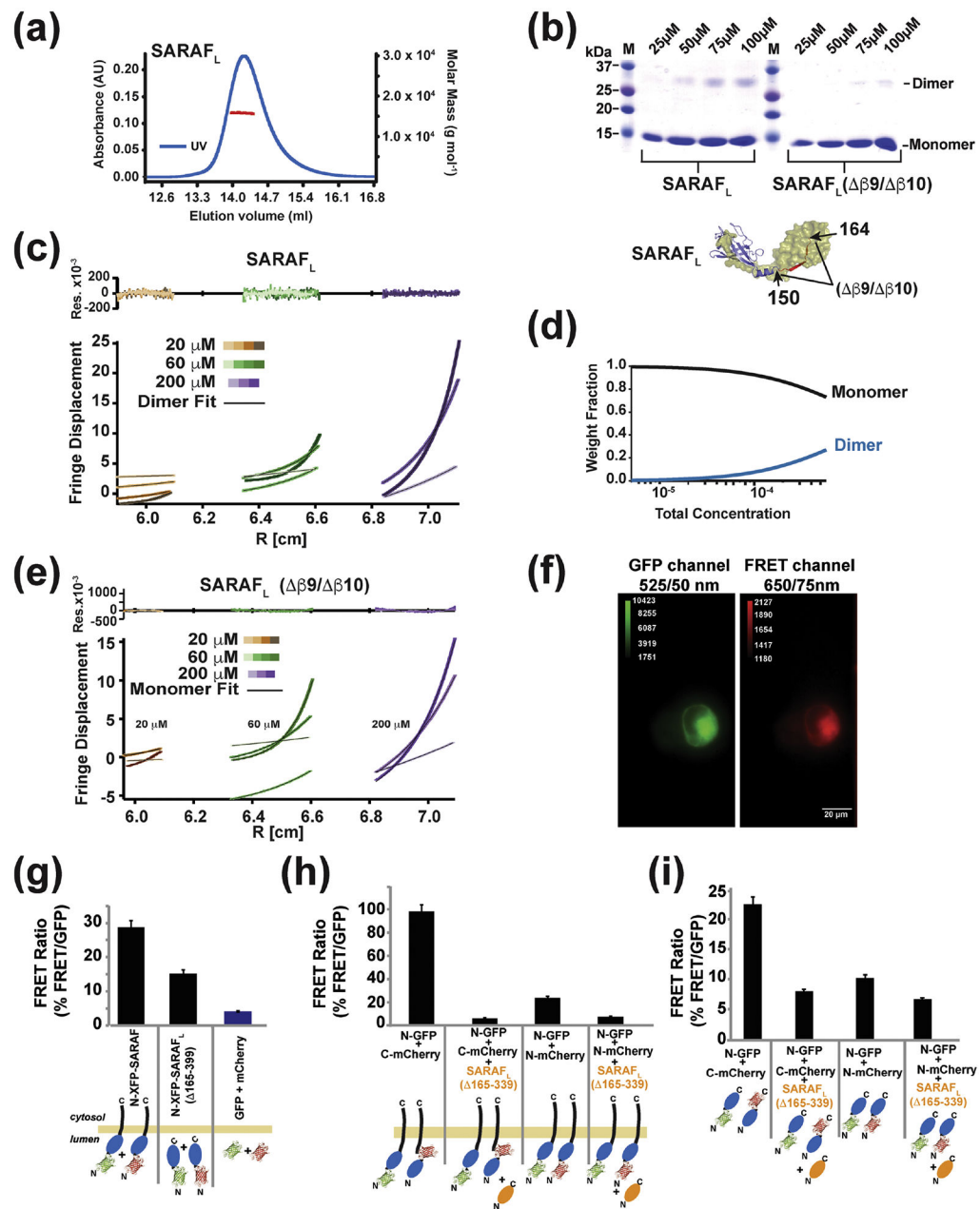


Fig. 5. SARAF self-association requires the SARAF luminal switch domain

(a) SEC-MALS of 64 μM (1 mg ml⁻¹) SARAF_L (experimental Mw 15.84 kDa ± 0.08, Mw/Mn = 1.000 ± 0.007, predicted monomer Mw 15.49 kDa). (b) SDS-PAGE of glutaraldehyde crosslinked SARAF_L and SARAF_L (Δβ9/Δβ10) as a function of protein concentration indicates SARAF_L dimerization. (c) Equilibrium ultracentrifugation of SARAF_L at the indicated concentrations. Rotor speeds of 10K, 18K, 22K and 31K rpm are denoted by increasingly darker shades for each concentration. Residuals show fits to a monomer-dimer self-association model. (d) Calculated fraction of monomer and dimer SARAF_L species as a function of concentration. (e) Equilibrium ultracentrifugation of SARAF_L (Δβ9/Δβ10) at the indicated concentrations. Rotor speeds of 10K, 18K, 22K and

31K rpm are denoted by increasingly darker shades for each concentration. Residuals show fits to a single species model. **(f)** Example of images taken of cells expressing GFP-SARAF and mCherry-SARAF using DualView. The red channel is the FRET signal. **(g)** Bar graph describing the FRET/GFP signal ratio of acquired images as described in **(f)**. Fluorescent tags are fused N-terminally to SARAF or SP-SARAF_L-R (SARAF luminal domain (165–339) with a signal peptide, SP, and an ER retention signal, R). Signals from cells expressing monomeric SP-GFP-R and SP-mCherry-R are used to establish the background signal. **(h)** SP-SARAF_L-R (orange) inhibits the FRET signals between XFP-SARAF and **(i)** N-terminally tagged, SP-XFP-SARAF_L-R, or C-terminally tagged, SP-SARAF_L-XFP-R, luminal domains. For (g-i) *** denotes $p < 0.001$. n for each combination is denoted above the bars.

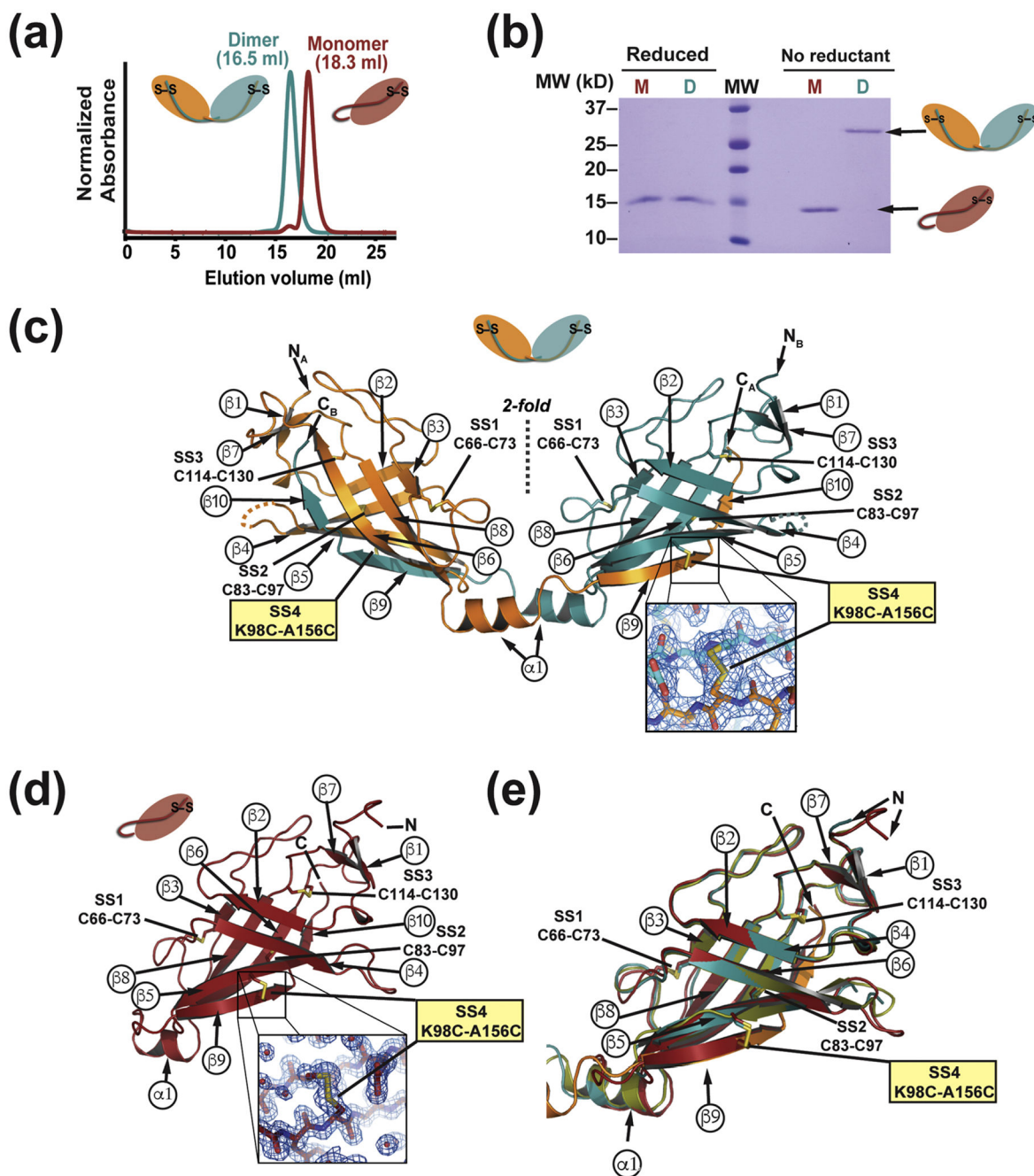


Fig. 6. Characterization and structures of Cys-locked SARAF_L mutants

(a) Size exclusion chromatography profiles monomer and dimer species of SARAF_L K98C/A156C. The Cys-locked dimer species elution profile is shifted earlier, consistent with a larger hydrodynamic radius. **(b)** SDS-PAGE gel of purified SARAF_L K98C/A156C monomer (M) and dimer (D) species. The dimer band collapses to the same size as the monomer band upon addition of reducing agent (β ME). **(c)** Crystal structure of the Cys-locked SARAF_L K98C/A156C dimer showing the same topology and disulfide bonding as wild type SARAF_L. Inset shows electron density (blue mesh, 1.5 β) for the engineered extra 4th disulfide bond (SS4). **(d)** Crystal structure of the Cys-locked SARAF_L K98C/A156C

monomer again showing the same strand arrangement and topology as wild type SARAF_L with the exception of β 9 and β 10 inserting in cis into the monomer β -sheet. Inset shows electron density (blue mesh, 1.5 β) for the engineered 4th disulfide bond (SS4). **(e)** Superposition of wild type SARAF_L (smudge green), Cys- locked SARAF_L K98C/A156C dimer protomers (orange and deep teal) and Cys-locked SARAF_L K98C/A156C monomer (firebrick red) showing the fold conservation across all three structures.

Author Manuscript

Author Manuscript

Author Manuscript

Author Manuscript

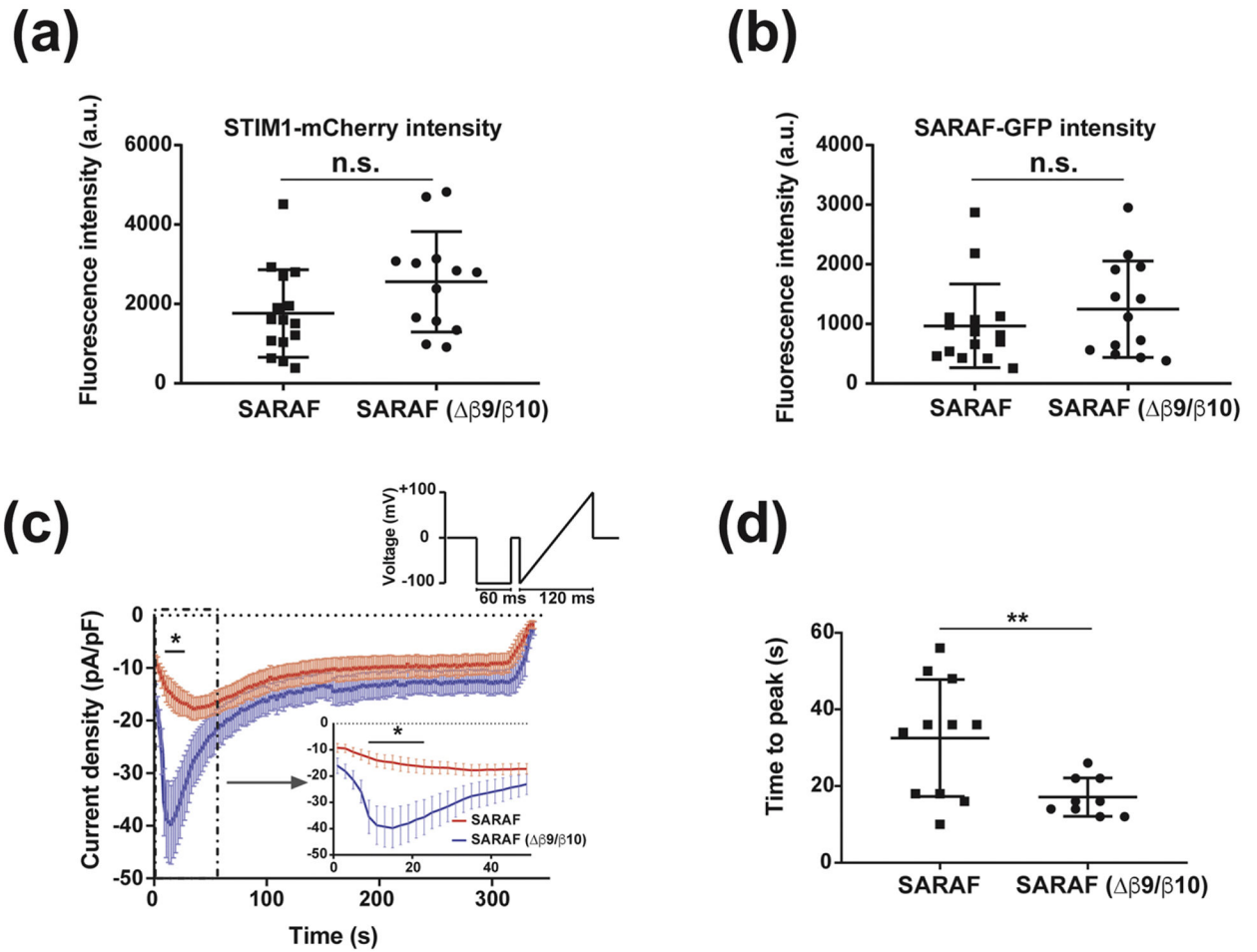


Fig. 7. Self-associated SARAF accelerates SOCE inactivation

(a) STIM1-mCherry and (b) SARAF-GFP expression measured by fluorescence using epifluorescence illumination of cells expressing Ora1-CFP, STIM1-mCherry and SARAF-GFP or SARAF ($\Delta\beta 9/\beta 10$)-GFP. (c) Average La^{3+} -sensitive current densities of HEK293 cells expressing Ora1-CFP, STIM1-mCherry, and SARAF-GFP or SARAF ($\Delta\beta 9/\beta 10$)-GFP measured at the end of 60 ms hyperpolarizing pulse to -100 mV in the presence of 10 mM extracellular Ca^{2+} . Inset shows the first 50s of recording. Stimulation protocol is shown and was applied at 0.5 Hz. (d), Time to peak measured following the application of 10 mM Ca^{2+} for SARAF and SARAF ($\Delta\beta 9/\beta 10$). $n = 11$ and 9, respectively. "*" indicates $p < 0.05$. "**" indicates $p < 0.01$. n.s., not statistically different. Error bars indicate s.e.m.